Field Observations of Wave-Induced Streaming through a Submerged Seagrass (Posidonia Oceanica) Meadow

Citation: Luhar, Mitul et al "Field Observations of Wave-Induced Streaming through a Submerged Seagrass (Posidonia Oceanica) Meadow." Journal of Geophysical Research: Oceans 118, 4 (April 2013): 1955–1968 © 2013 American Geophysical Union

As Published: http://dx.doi.org/10.1002/JGRC.20162

Publisher: American Geophysical Union (AGU)

Persistent URL: http://hdl.handle.net/1721.1/117409

Version: Final published version: final published article, as it appeared in a journal, conference proceedings, or other formally published context

JOURNAL OF GEOPHYSICAL RESEARCH: OCEANS, VOL. 118, 1955–1968, doi:10.1002/jgrc.20162, 2013

Field observations of wave-induced streaming through a submerged seagrass (*Posidonia oceanica*) meadow

Mitul Luhar,[1] Eduardo Infantes,[2] Alejandro Orfila,[2] Jorge Terrados,[2] and Heidi M. Nepf[1]

Received 24 October 2012; revised 25 February 2013; accepted 11 March 2013; published 11 April 2013.

[1] This paper reports the findings of a 2 week field campaign designed to study wave-induced flows within a meadow of *Posidonia oceanica* at water depth 9 *m*. Previous laboratory experiments suggest that waves induce a mean mass drift in the direction of wave propagation ("streaming") through submerged canopies of vegetation. This paper provides the first field measurements of this wave-induced streaming. During periods of high wave activity, streaming flows with magnitudes as high as 20% of the near-bed oscillatory velocity were measured within the meadow. In addition to presenting field measurements of wave-induced streaming, this paper also considers the damping of wave-induced oscillatory flow within the seagrass meadow. Oscillatory velocities measured within the meadow were reduced by less than 30% relative to those above the meadow over the duration of the study. This is in agreement with previous laboratory and field measurements which show that oscillatory flows are damped less within submerged canopies compared to unidirectional flows. Existing analytical models underpredict the magnitude of the streaming flow and overpredict oscillatory velocity reductions. These discrepancies are thought to arise because the drag generated by flexible seagrasses moving with wave-induced flow is not well described.

Citation: Luhar, M., E. Infantes, A. Orfila, J. Terrados, and H. M. Nepf (2013), Field observations of wave-induced streaming through a submerged seagrass (*Posidonia oceanica*) meadow, *J. Geophys. Res. Oceans*, *118*, 1955–1968, doi:10.1002/jgrc.20162.

1. Introduction

[2] Many of the ecosystem services provided by seagrasses stem from their ability to modify the local hydrodynamic environment [*Bouma et al*., 2005]. For example, by reducing the near-bed flow and limiting sediment resuspension, seagrasses stabilize the seabed [*Fonseca and Cahalan*, 1992; *Gacia et al*., 1999] and provide shelter for fauna [*Irlandi and Peterson*, 1991]. A reduction in sediment suspension also improves water clarity, thereby increasing light penetration into the water column and boosting primary productivity [*Ward et al*., 1984]. Further, by trapping the organic matter associated with sediment runoff and that associated with the local decay of plant roots, rhizomes, and leaves, seagrass meadows act as important carbon sinks [see, e.g., *Nelleman et al*., 2009]. Finally, the rate of water renewal within the meadow can limit nutrient and oxygen transfer. In addition to being critical to the health of the seagrasses themselves, nutrient cycling and oxygen production are two of the most valuable ecosystem services [*Costanza et al*., 1997] provided by seagrass meadows.

[3] Given its environmental significance, the physics of flow-vegetation interaction has received significant attention. The flow within, above, and around vegetated canopies has been successfully described for unidirectional currents (for recent reviews, see, e.g., *Nepf*, 2012; *Luhar and Nepf*, 2013]. However, for many seagrass meadows, wave-induced oscillatory flows, rather than unidirectional currents, are the dominant hydrodynamic forcing. Thus far, the primary aim for most wave studies has been to quantify wave energy dissipation over seagrass meadows [*Fonseca and Cahalan*, 1992; *Kobayashi et al*., 1993; *Bradley and Houser*, 2009; *Infantes et al*., 2012]. Nevertheless, some recent studies have also described wave-induced oscillatory flows within and above submerged canopies [*Lowe et al*., 2005; *Lowe et al*., 2007; *Luhar et al*., 2010].

[4] Based on theoretical considerations and laboratory experiments employing a model canopy of rigid cylinders, *Lowe et al*. [2005] showed that unlike unidirectional flow, wave-induced oscillatory flow within the canopy is not significantly damped relative to that above the canopy. The laboratory measurements presented in *Luhar et al*. [2010] showed that this also holds for flexible model vegetation. Specifically, *Luhar et al*. [2010] found that within similar model canopies, unidirectional flows were reduced by as much as 80% relative to the flow above the canopy, while wave-induced oscillatory flows were reduced by

[1]Department of Civil and Environmental Engineering, Massachusetts Institute of Technology, Cambridge, Massachusetts, USA.
[2]Instituto Mediterráneo de Estudios Avanzados, IMEDEA (CSIC-UIB), Esporles, Mallorca, Spain.

Corresponding author: M. Luhar, Department of Civil and Environmental Engineering, Massachusetts Institute of Technology, 77 Massachusetts Avenue, 48-216, Cambridge, MA 02139, USA. (mluhar@alum.mit.edu)

2169-9275/13/10.1002/jgrc.20162

≤20%. Notably, *Luhar et al*. [2010] also revealed the presence of a wave-induced mean mass drift in the direction of wave propagation ("streaming") within the meadow and developed a simple theoretical model that explains the streaming. This model proposes that the streaming flow is driven by a nonzero wave stress, similar to the streaming observed in wave boundary layers. *Luhar et al*. [2010] also hypothesized that for flexible plants, the streamwise bias in posture created by the streaming flow could lead to a drag asymmetry (i.e., higher drag under wave trough and lower drag under wave crest) that reinforces the mean streaming flow. In the present paper, we explore the impact of drag asymmetry on the streaming flow in greater detail.

[5] Field confirmation for the laboratory findings of *Lowe et al*. [2005] and *Luhar et al*. [2010] has thus far been limited. Existing field measurements do provide some evidence that oscillatory flows are damped less than mean currents within submerged canopies of vegetation. For example, *Koch and Gust* [1999] reported that velocities within seagrass beds were reduced by ~70% at a tide-dominated site and by ~40% at a wave-dominated site. In a recent study, *Hansen and Reidenbach* [2012] showed that near-bottom mean velocities were reduced by as much as 90% within seagrass beds, while wave orbital velocities were only reduced by 20% compared to the flow above the seagrass bed. Similarly, velocity measurements made by *Andersen et al*. [1996] within and above a kelp forest also showed that wave-induced velocities were damped by less than 10% within the vegetated canopy. *Thomas and Cornelisen* [2003] reported that ammonium uptake was enhanced in seagrass beds for oscillatory flows compared to unidirectional flows. Since uptake increases with velocity, these measurements could be explained by the fact that oscillatory flows are damped less in seagrass beds.

[6] To our knowledge, there are no previous field observations of wave-induced streaming through submerged canopies. This can perhaps be attributed to the fact that most existing field measurements have been carried out in relatively shallow environments with depths <2 m or in regions with strong tides [*Koch and Gust*, 1999; *Bradley and Houser*, 2009; *Hansen and Reidenbach*, 2012]. In such environments, any wave-induced streaming flow may be masked by wind-driven or tidal currents. Further, if the seagrass canopy occupies a large fraction of the water column (i.e., for shallow flows), the presence of a surface setup driven return flow can limit the magnitude and vertical extent of any wave-induced streaming. The purpose of the present study is to document wave-induced streaming in the field, providing field confirmation for the laboratory measurements of *Luhar et al*. [2010]. For this purpose, we selected a site at which other near-bed currents are minimized.

[7] Below, we report the findings of a 2 week field campaign designed to study wave-induced flows within, and above, a canopy of the seagrass *Posidonia oceanica* in water depth 9 *m* (cf. <2 *m* for previous studies). Our measurements confirm the presence of a wave-induced mean mass drift in the direction of wave propagation during periods of high wave activity. Because this mean current introduces a directional bias, it could have profound implications for the transport of suspended sediment and organic material. The mean mass drift could also be an important mechanism of water renewal within the meadow (in addition to turbulent exchange between the meadow and overlying water). We also consider the fractional reduction of wave-induced oscillatory flow within the vegetated canopy. Our measurements provide further evidence that oscillatory flow within the canopy is not significantly reduced relative to that above the canopy. Finally, we present quantitative comparisons between our measurements of flow reduction and wave-induced streaming, and the model predictions from *Lowe et al*. [2005] and *Luhar et al*. [2010], respectively.

2. Theory

[8] In this section, we provide a brief review of the model developed by *Lowe et al*. [2005] to predict the in-canopy oscillatory velocity reduction and the model developed by *Luhar et al*. [2010] to predict the magnitude of the wave-induced streaming flow. In addition, we extend the streaming flow model to account for the plant posture bias observed by *Luhar et al*. [2010]. We show that the drag asymmetry created by this posture bias can strengthen the mean streaming flow.

2.1. Oscillatory Flow Reduction

[9] *Lowe et al*. [2005] and *Luhar et al*. [2010] showed that the degree to which oscillatory velocities are damped within submerged meadows depends on the relative importance of three forces: the shear force generated at the top of the meadow, the vegetation drag, and the inertial forces (including added mass). These forces are characterized by the following three length scales: (i) the shear length scale,

$$L_S = \frac{2h_v}{C_f} \tag{1}$$

where h_v is the height of the canopy and $C_f = O(0.01–0.1)$ is the meadow friction factor; (ii) the drag length scale,

$$L_D = \frac{2h_v(1-\lambda_p)}{C_D\lambda_f} \tag{2}$$

where λ_p and λ_f are the planar area per unit bed area and frontal area per unit bed area for the meadow, respectively, and $C_D = O(1)$ is the vegetation drag coefficient; and (iii) the oscillation length scale, which is the wave orbital excursion above the meadow,

$$A_w = \frac{U_w}{\omega} \tag{3}$$

Here U_w is the amplitude of the oscillatory velocity, and ω is the wave frequency.

[10] The frontal area per unit bed area for the submerged canopy can be expressed as $\lambda_f = a_v h_v$, where a_v is the vegetation frontal area per unit volume [see, e.g., *Luhar et al*., 2008]. When the wave excursion is much smaller than the drag and shear length scales, $A_w \ll (L_S, L_D)$, the wave motion is unaffected by vegetation drag and shear, and inertial forces dominate. Drag and shear become important when the wave excursion is

greater than the length scales representing these forces, $A_w > (L_S, L_D)$. At the limit $A_w \gg (L_S, L_D)$, inertial forces become unimportant.

[11] At the inertia-dominated limit, $A_w \ll (L_S, L_D)$, the oscillatory velocity within the meadow, $U_{w,m}$, is not reduced significantly relative to that above the meadow, U_w, and the ratio of the two velocities is [*Lowe et al*., 2005; *Luhar et al*., 2010]

$$\alpha_i = \frac{U_{w,m}}{U_w} = \frac{1-\lambda_p}{1+(C_m-1)\lambda_p} \tag{4}$$

Here C_m is the added mass coefficient for the vegetation [see, e.g., *Vogel*, 1994]. Throughout this paper, the variable U_w refers to amplitude of the oscillatory velocity above the meadow. A subscript m is used for in-meadow velocities (e.g., $U_{w,m}$). For low-frequency waves, with $A_w \gg (L_S, L_D)$, inertial forces are negligible and the velocity ratio is set by a balance between the shear force and vegetation drag:

$$\alpha_c = \frac{U_{w,m}}{U_w} = \sqrt{\frac{L_D}{L_S}} = \sqrt{\frac{C_f(1-\lambda_p)}{C_D\lambda_f}} \tag{5}$$

This low frequency limit essentially resembles a unidirectional current (i.e., zero frequency, subscript c denotes current limit), for which the velocity within the meadow is significantly damped [see, e.g., *Ghisalberti and Nepf*, 2006]. In general, α_i and α_c represent upper and lower bounds, respectively, for the velocity ratio. For intermediate cases, with $A_w = O(L_S, L_D)$, the velocity ratio is expected to fall between α_i and α_c. Finally, note the ratios given by equations (4) and (5) correspond to the depth-averaged velocity within the meadow, $U_{w,m}$, normalized by the velocity immediately above the meadow, U_w [*Lowe et al*., 2005; *Luhar et al*., 2010].

2.2. Wave-Induced Streaming

[12] As noted above, laboratory measurements made by *Luhar et al*. [2010] revealed the presence of a mean mass drift within the meadow, in the direction of wave propagation. *Luhar et al*. [2010] developed a simple momentum- and energy-balance model that successfully predicted the magnitude of the mean currents, $U_{c,m}$, measured in the laboratory. This model is based on the hypothesis that the mass drift is driven by a nonzero wave stress, similar to the streaming observed in wave boundary layers. The model assumes that energy is transferred into the meadow primarily via the work done by the wave-induced pressure at the top of the meadow, $-\overline{p_w w_w}$, where p_w is the pressure and w_w is the vertical velocity at the top of the meadow, and the overbar denotes a time average. This energy transfer is balanced by dissipation within the meadow, $\overline{E_D}$, leading to

$$-\overline{p_w w_w} \approx \overline{E_D} \tag{6}$$

Assuming that linear wave theory holds above the meadow, the pressure field is given by $p_w = \rho(\omega/k)u_w$, where ρ is the density of water, k is the wave number, and $u_w(t)$ is the horizontal oscillatory velocity (note that U_w is the magnitude of the time-varying, oscillatory velocity u_w). This yields the wave stress

$$-\overline{\rho u_w w_w} \approx \frac{k}{\omega}\overline{E_D} \tag{7}$$

which represents a time-averaged transfer of momentum into the meadow. In turn, this transfer of momentum into the meadow is balanced by the time-averaged drag force, $\overline{F_D}$:

$$-\overline{\rho u_w w_w} \approx \frac{k}{\omega}\overline{E_D} \approx \overline{F_D} \tag{8}$$

[13] According to convention, the drag (per unit volume) generated by seagrass meadows in combined wave-current flows should be expressed as $(1/2)\rho C_D a_v |U_{c,m} + u_{w,m}| (U_{c,m} + u_{w,m})$. However, experimental [*Sarpkaya and Isaacson*, 1981] and numerical [*Zhou and Graham*, 2000] studies have shown that a two-term formulation with separate drag coefficients for the mean and oscillatory components of flow, $(1/2)\rho a_v\left(C_{Dc}U_{c,m}^2 + C_{Dw}|u_{w,m}|u_{w,m}\right)$, provides a better fit to the observations compared to the conventional quadratic law. Here C_{Dc} and C_{Dw} are the distinct current- and wave-drag coefficients, respectively.

[14] With this two-term formulation, *Luhar et al*. [2010] made two additional assumptions to arrive at an estimate for the mean mass drift. First, that wave energy dissipation in the meadow is dominated by the wave component of drag, $\overline{E_D} \approx \overline{\int_0^{h_v} \frac{1}{2}\rho C_{Dw} a_v |u_{w,m}| u_{w,m}^2 dz}$, where $u_{w,m}(t)$ is the oscillatory velocity within the meadow of magnitude $U_{w,m}$. Second, that the time-averaged drag force is due to the mean current generated in the meadow, $\overline{F_D} \approx \overline{\int_0^{h_v} \frac{1}{2}\rho C_{Dc} a_v U_{c,m}^2 dz}$. With these simplifications, equation (8) yields the following prediction for the wave-induced streaming velocity:

$$U_{c,m} \approx \sqrt{\frac{4k}{3\pi\omega}\frac{C_{Dw}}{C_{Dc}}U_{w,m}^3} \tag{9}$$

Equation (9) successfully predicted the streaming velocities measured by *Luhar et al*. [2010], with the ratio of drag coefficients assumed to be $C_{Dw}/C_{Dc} = 1$, as suggested by *Zhou and Graham* [2000].

[15] Note that we employ three different drag coefficients in this study. The drag length scale, L_D, (equation (2)) is defined in terms of a general drag coefficient, C_D, while the predicted streaming velocity in equation (9) employs distinct wave and current drag coefficients, C_{Dw} and C_{Dc}, respectively. Strictly, because equations (1)–(5) consider wave-induced oscillatory flows, $C_D = C_{Dw}$ in equation (2). Nevertheless, since we also consider the large excursion limit (equation (5)), where the wave-induced flow resembles a unidirectional current, we employ a general drag coefficient, C_D, in our definition of the drag length scale, L_D (equation (2)).

2.3. Effect of Plant Posture Bias on Streaming

[16] *Luhar et al*. [2010] observed that the wave-induced mean current led to an asymmetry in posture for their model plants, whereby the blades lay streamwise in the direction of wave propagation under the wave crest and remained more upright under the wave trough. Thus, the frontal area of the meadow ($a_v h_v$) is effectively smaller under the wave

crest and larger under the trough, leading to an asymmetry in drag ($\sim C_{Dw}a_v h_v|u_{w,m}|u_{w,m}$). The drag asymmetry created by this posture bias (i.e., lower drag under wave crest and higher drag under wave trough) can reinforce the streaming flow. To account for this effect, we propose a simple extension to the model developed by *Luhar et al*. [2010].

[17] Assuming that the in-canopy velocity and canopy geometry do not vary significantly over canopy height, the drag generated by the canopy is $F_D = (1/2)\rho a_v h_v \left(C_{Dw}|u_{w,m}(t)|u_{w,m}(t) + C_{Dc}U_{c,m}^2 \right)$. As before, $u_{w,m}(t) = U_{w,m}\sin\ \omega t$ is the in-canopy oscillatory velocity and $U_{c,m}$ is the mean current. To account for the change in frontal area, we replace the constant factor $a_v h_v$ with $a_v h_v(1 - \epsilon \sin\omega t)$, which leads to

$$F_D = \frac{1}{2}\rho a_v h_v (1 - \epsilon \sin\omega t)\left(C_{Dw}|u_{w,m}|u_{w,m} + C_{Dc}U_{c,m}^2 \right) \quad (10)$$

Here $\epsilon\ (> 0)$ represents the degree of asymmetry. The assumed time variation in frontal area, $(1 - \epsilon \sin\omega t)$, ensures that the frontal area is lowest when the wave velocity, $u_{w,m}$, is highest and positive (i.e., right under the wave crest). With this modification, the time-averaged drag force becomes

$$\overline{F_D} = \frac{1}{2}\rho a_v h_v \left(C_{Dc}U_{c,m}^2 - \frac{4}{3\pi}\epsilon C_{Dw}U_{w,m}^2 \right) \quad (11)$$

Equation (11) indicates that the posture bias generates an additional drag force (second term in equation (11)), which is in the opposite sense to the drag generated by the streaming flow (first term in equation (11)). This additional term arises because the frontal area is larger under the wave trough ($u_{w,m} < 0$) compared to the wave crest ($u_{w,m} > 0$), and so greater drag is generated under the wave trough.

[18] In addition to modifying the time-averaged drag force, a posture bias also affects the energy dissipation within the meadow, $\bar{E_D}$, which determines the magnitude of the wave stress (equation (7)). Accounting for the time-varying frontal area, it can be shown that the dissipation rate becomes

$$\begin{aligned} \overline{E_D} &= \overline{F_D(u_{w,m} + U_{c,m})} \\ &= \frac{1}{2}\rho a_v h_v C_{Dw} U_{w,m}^3 \frac{4}{3\pi}\left(1 - \epsilon\frac{U_{c,m}}{U_{w,m}} \right) \end{aligned} \quad (12)$$

Equation (12) indicates that the posture bias leads to a decrease in the dissipation rate. Note that to arrive at equation (12), both the posture asymmetry, ϵ, and the ratio of the streaming flow to the oscillatory flow, $U_{c,m}/U_{w,m}$, were assumed to be small ($\ll 1$). Only terms up to quadratic in these two factors were retained. With these modified expressions for drag (equation (11)) and energy dissipation (equation (12)), the mean momentum balance for the meadow shown in equation (8) leads to the following prediction for the mean streaming flow:

$$\left(\frac{U_{c,m}}{U_{w,m}} \right)^2 = \frac{4}{3\pi}\left(\frac{C_{Dw}}{C_{Dc}} \right)\left[\frac{kU_{w,m}}{\omega}\left(1 - \epsilon\frac{U_{c,m}}{U_{w,m}} \right) + \epsilon \right] \quad (13)$$

[19] For zero posture bias ($\epsilon = 0$), equation (13) yields the same prediction for the mean streaming flow as the model developed by *Luhar et al*. [2010] (equation (9)). However, for $\epsilon > 0$, equation (13) suggests that there are two different mechanisms driving the mean streaming flow. The first term inside the square brackets represents the streaming flow generated by the wave stress, while the second term represents the streaming flow driven by the drag asymmetry. The relative contributions of the wave stress and the drag asymmetry terms depend on the relative magnitudes of $(kU_{w,m}/\omega)$ and ϵ. Compared to the zero-bias case, a biased posture leads to a reduction in the wave stress driven streaming flow. This is because the wave stress is proportional to the rate of energy dissipation within the meadow (equation (7)), which is reduced by the posture bias (equation (12)). However, the additional streaming flow contribution due to the drag asymmetry compensates for this reduction. Specifically, the wave stress contribution is reduced by a factor $\propto \left(kU_{c,m}/\omega\right)\epsilon$, while the additional contribution due to drag asymmetry is $\propto \epsilon$. For both laboratory and field conditions, the streaming velocity, $U_{c,m}$, is likely to be at least an order of magnitude smaller than the wave celerity, ω/k, such that $(kU_{c,m}/\omega) \ll 1$. Therefore, the net effect of a posture bias ϵ on the mean streaming flow is positive.

[20] Note that equations (10)–(13) were derived based on the assumption that the frontal area, $a_v h_v \sim (1 - \epsilon \sin\omega t)$, is lowest when the wave velocity, $u_{w,m} \sim \sin\omega t$, is highest, i.e., directly under the crest. However, it can be shown that equations (10)–(13) also hold for the more general case with an arbitrary phase shift (ϕ) between the posture bias and the wave velocity, i.e., $a_v h_v \sim [1 - \epsilon \sin(\omega t + \phi)]$. For this more general case, an effective posture bias, $\epsilon\cos\phi$, must be used in equation (13) instead of ϵ. As long as the frontal area is greater on average under the wave trough, $\epsilon\cos\phi > 0$, the posture bias serves to strengthen the streaming flow. For the relatively unphysical case where the frontal area is greater under the wave crest ($\epsilon\cos\phi < 0$), the posture bias weakens the streaming flow, and negative streaming velocities (i.e., against the direction of wave propagation) are possible. For $\epsilon\cos\phi < 0$, the factor $U_{c,m}^2$ on the left-hand side of equation (13) must be replaced with $|U_{c,m}|U_{c,m}$ to account for the possibility of negative streaming.

3. Methods

[21] This field study was conducted in Cala Millor located on the eastern coast of Mallorca, one of the Balearic Islands in the Mediterranean Sea (Figure 1). Cala Millor is an intermediate barred sandy beach in an open, microtidal bay (spring tidal range <0.25 m). The bay has an area of approximately 14 km^2 and is exposed to incoming wind and waves from the Northeast to East-southeast directions (Figure 1). Based on propagations from 44 years of hourly wave data, *Gomez-Pujol et al*. [2007] suggest that the mean wave height in Cala Millor at water depth 5 m varies between 0.2 m (April–September) and 0.4 m (October–March), while the peak period ranges from 4.7 s (April–September) to 7.0 s (October–March). However, this area is subject to cyclogenetic activity throughout the year, and so wave heights and peak periods significantly greater than these mean values are common (see, e.g., measurements in Figure 2).

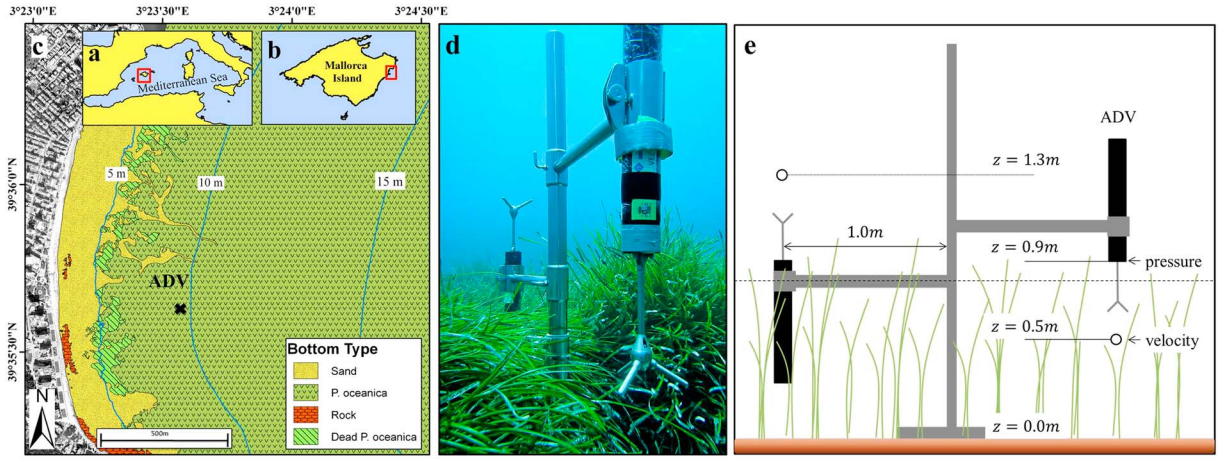

Figure 1. Field study location and setup. (a–c) Maps showing field site location. (c) Depth contours and bottom type at the site. The measurement location is marked with an "x." (d) Photograph showing ADV setup (credit: Eduardo Infantes). (e) Schematic showing stainless steel structure and ADV setup (not to scale). The velocity measurement locations are marked with a circle. The horizontal dashed line indicates the mean shoot length, $l_v = 0.8$ m.

[22] Within the bay, the seagrass *Posidonia oceanica*, a species endemic to the Mediterranean Sea, forms an extensive meadow at depths between 6 m and 35 m [*Infantes et al*., 2009]. Note that the western Mediterranean presents a relatively clear water environment, which makes the presence of photosynthetic plants viable at such depths. *Infantes et al*. [2009] suggest that the upper depth limit for the meadow (6 m) is set by near-bottom orbital velocities associated with mean wave conditions rising above $0.4\ \mathrm{m\,s^{-1}}$. At depths less than 6 m, the bottom substrate in the bay is primarily sand with some outcroppings of rock. In a recent study, *Infantes et al*. [2012] reported the following seagrass meadow properties for the same location: mean shoot density, $n = 620 \pm 30\ \mathrm{m^{-2}}$, mean shoot length, $l_v = 0.8 \pm 0.1$ m, and an average leaf area of $a_v' = 210 \pm 20\ \mathrm{cm^2}$ per shoot. Following *Luhar et al*. [2010], the seagrass frontal

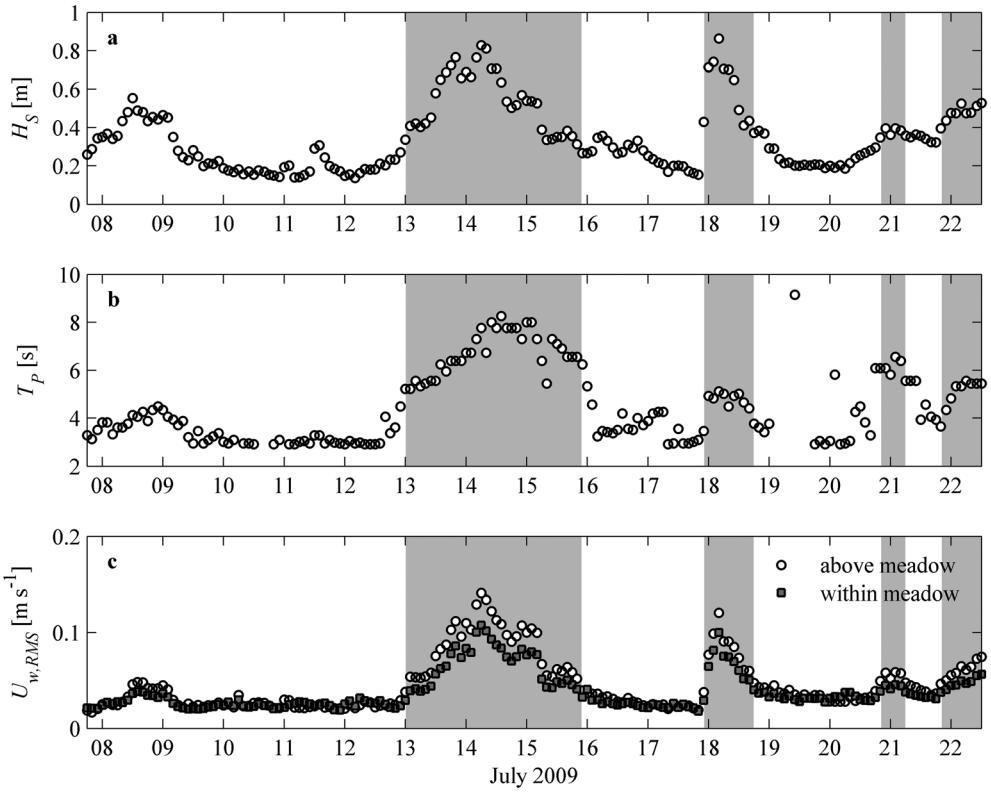

Figure 2. (a) Significant wave height, H_S, and (b) peak period, T_P, estimated from velocity measurements made above the meadow. (c) RMS horizontal velocities within and above the meadow. The shaded regions indicate periods of high wave activity, with $U_{w,RMS} > 0.05\ \mathrm{m\ s^{-1}}$ above the meadow.

area per unit bed area is therefore $\lambda_f = na_v' = 13 \pm 2$, and assuming a typical blade thickness of $t_v = 0.5$ mm [*Marbà et al.*, 1996], the seagrass planar area per unit bed area is $\lambda_p = na_v' t_v / l_v = 0.008 \pm 0.001$.

[23] Two self-contained Acoustic Doppler Velocimeters (ADVs, Nortek Vector) were used to make pressure and velocity measurements at a water depth of $h = 9$ m from 7 to 23 July 2009. The measurement location is shown in Figures 1a–1c. As discussed in the introduction, most existing velocity measurements in seagrass meadows have been performed in shallow water of depth <2 m [*Koch and Gust*, 1999; *Bradley and Houser*, 2009; *Hansen and Reidenbach*, 2012]. So, our measurements, obtained in water depth 9 m and at a location largely free of tidal flow, represent a unique dataset. The ADVs were mounted on a stainless steel structure comprising a vertical pole and two horizontal arms. An upward-facing ADV measured velocity above the seagrass meadow at a height $z = 1.3$ m above the bed, and a downward-facing ADV measured velocity within the meadow at $z = 0.5$ m (Figures 1d and 1e). The pressure sensors for both ADVs were located approximately 0.9 m above the sea bed. Pressure and velocity were measured in bursts of 15 min every 2 h at a sampling frequency of 4 Hz (i.e., $M_s = 3600$ samples in each burst). Each ADV was equipped with a built-in compass and tilt sensor. Velocities were recorded in an East-North-Vertical reference frame. Since the contours of bed elevation (and the shoreline; Figure 1) are oriented roughly North-South at the measurement location, we consider East-West to be the cross-shore direction.

[24] For each burst, we calculated the mean (i.e., time averaged) East and North velocities, E_c and N_c, respectively, above and within the seagrass meadow as the average of all individual samples (E_j and N_j) in the burst, e.g.,

$$E_c = \frac{1}{M_s}\sum_{j=1}^{M_s} E_j \tag{14}$$

The mean velocities were then subtracted from the record to calculate root-mean-square (RMS) oscillatory velocities, e.g.,

$$E_{w,RMS} = \sqrt{\frac{1}{M_s}\sum_{j=1}^{M_s}\left(E_j - E_c\right)^2} \tag{15}$$

We use the variables U_c and U_w to refer to total mean and oscillatory horizontal velocities. That is, $|U_c| = \sqrt{E_c^2 + N_c^2}$ and $|U_{w,RMS}| = \sqrt{E_{w,RMS}^2 + N_{w,RMS}^2}$. The magnitude of the wave-induced oscillatory velocities was calculated from the measured RMS velocities assuming perfect sinusoids, i.e., $U_w = \sqrt{2}U_{w,RMS}$.

[25] The significant wave height, H_S, and peak wave period, T_P, for each burst were estimated from the velocity measurements using the following procedure. First, the spectral densities, S_E and S_N, for the East and North velocities were calculated using Welch's method (MATLAB, MathWorks, Inc.). The velocity spectra were then scaled to represent a surface elevation spectrum, S_H, assuming linear wave theory:

$$S_{Hj} = \left(S_{Ej} + S_{Nj}\right)\left(\frac{\sinh(k_j h)}{\omega_j \cosh(k_j z)}\right)^2 \tag{16}$$

Here S_{Hj}, S_{Ej}, and S_{Nj} refer to the spectral densities corresponding to frequency ω_j. As before, h is the water depth and z is the distance from the bed at which the velocity was measured. The peak period was estimated as $T_P = 2\pi/\omega_P$, where ω_P is the frequency corresponding to the peak in the surface elevation spectrum. Using the standard definition, the significant wave height was calculated as

$$H_S = 4\sqrt{\sum_j S_{Hj}\Delta\omega_j} \tag{17}$$

where $\Delta\omega_j$ is the bandwidth for frequency ω_j. Across all frequencies, the bandwidth was constant, $\Delta\omega_j = 0.0245$ rad s^{-1}, set by the sampling frequency and the algorithm used to calculate spectral densities.

[26] Laboratory measurements made by *Luhar et al.* [2010] show that above the meadow, oscillatory velocities are predicted reasonably well by linear wave theory. So, we estimated the significant wave height and peak period based on above-meadow ADV measurements. Since the velocities within the meadow are likely to be damped, we did not use the in-meadow measurements to calculate H_S and T_P. To limit the effect of any measurement noise on estimates of H_S and T_P, the surface elevation spectrum was limited to frequencies for which the amplification factor in equation (16), $\sinh^2(k_j h)/(\omega_j \cosh(k_j z))^2$, was smaller than 200. In effect, this restricts the spectrum to waves of period greater than $T = 2.9$ s. The chosen cutoff amplification factor (200) is somewhat arbitrary; however, it does not significantly affect the estimates for H_S. The significant wave height changes by less than 10% if the cutoff is chosen to be 100 or 400.

[27] Based on the reported accuracy for the ADVs, we estimate an instrument uncertainty of ± 0.005 m s^{-1}. Therefore, our subsequent analysis and discussion is limited to periods of high wave activity, with $U_{w,RMS} > 0.05$ m s^{-1}, so that the measurements are at least 10 times greater than the uncertainty. Finally, most field studies infer surface elevation spectra (equation (16)) from the measured dynamic pressure spectra [see, e.g., *Bradley and Houser*, 2009]. Using a procedure similar to the one described above, significant wave heights calculated based on pressure measurements, H_{SP}, showed good agreement with the velocity-based estimates, H_S. Specifically, over all measurement bursts, $H_{SP}/H_S = 1.06 \pm 0.08$ (mean $\pm$ s.d., $n_b = 178$).

4. Results

[28] Figure 2 shows the significant wave height, H_S, the peak period, T_P, and the RMS horizontal velocities within and above the meadow over the entire measurement period. The shaded regions indicate measurement periods with high wave activity, i.e., bursts with $U_{w,RMS} > 0.05$ m s^{-1}. This threshold corresponds roughly to bursts where wave heights exceeded $H_S > 0.35$ m. (Figure 2a), and peak periods exceeded $T_P > 4.5$ s (Figure 2b). We captured four such piods: on 13–16 July, 18 July, 20–21 July, and 22 July. Outside of these high wave periods, the estimated peak period

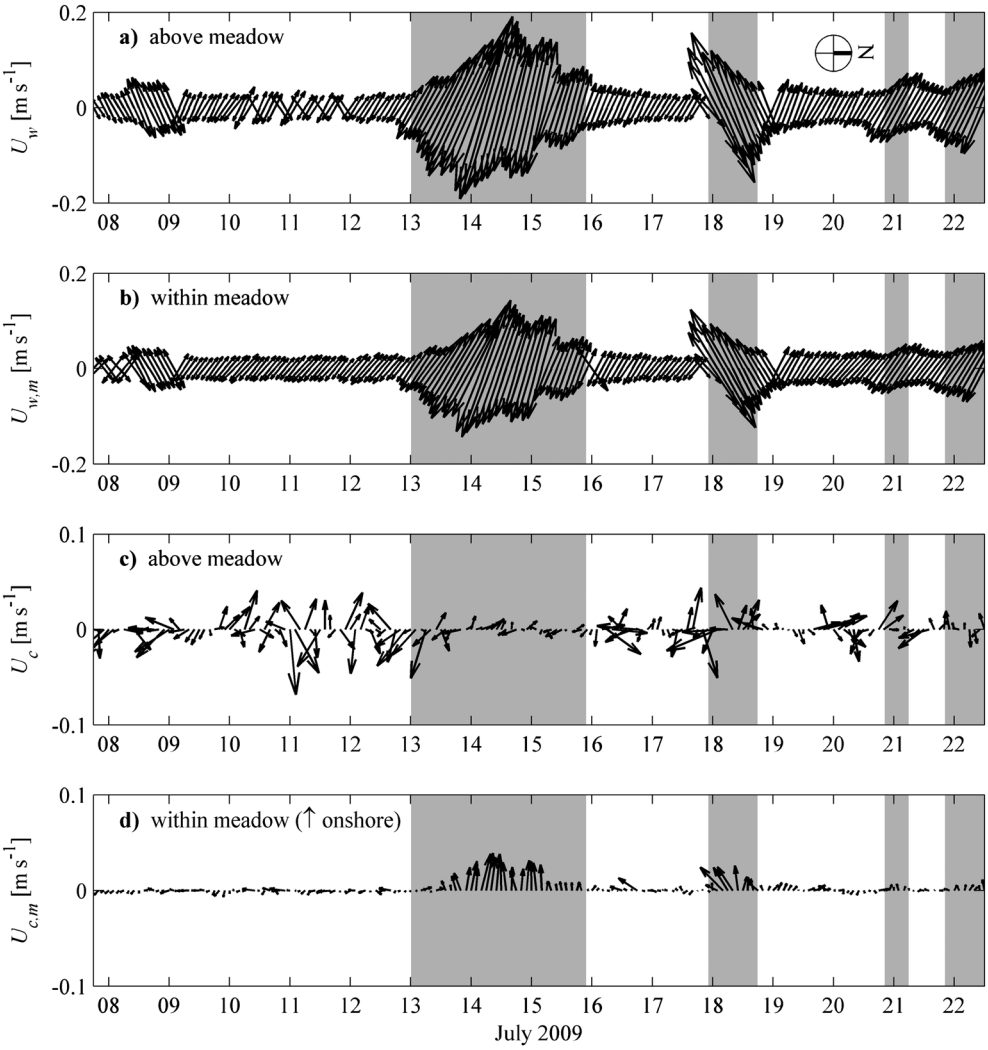

Figure 3. Wave velocities measured (a) above and (b) within meadow. The shaded regions indicate periods of high wave activity, with $U_{w,RMS} > 0.05$ m s^{-1} above the meadow. Mean velocities measured (c) above and (d) within meadow. North is as indicated in Figure 3a. Since the cross-shore direction is approximately East-West (Figure 1), onshore is upwards in this figure.

was typically $T_P \approx 3$ s, which is the cutoff frequency described earlier (Figure 2b; see, e.g., 10–12 July). For most of the measurement bursts (and all of the high wave periods), the RMS velocities measured within the canopy were reduced relative to those above the meadow (Figure 2c). Both the Eastern and Northern components of wave velocity measured within the meadow correlated well with those measured above the meadow (Figures 3a and 3b). However, Figures 3c and 3d show no such correlations for the mean currents. Even during measurement bursts where mean velocities exceeding $|U_c| > 0.05$ m s^{-1} were recorded above the meadow (Figure 3c; see, e.g., 10–12 July, the mean currents within the meadow were small, $|U_{c,m}| < 0.01$ m s^{-1}.

[29] Importantly, our measurements clearly show that a mean current in the direction of wave propagation (i.e., in the Westward, onshore direction) is generated within the meadow during periods of high wave activity (Figure 3d). For example, on 14 July, mean currents as large as $|U_{c,m}|$ 0.04 m s^{-1} (~20% of the oscillatory velocities) were measured in the onshore direction within the meadow, while the measured currents above the meadow were much smaller, $|U_c| < 0.02$ m s^{-1}. A visual comparison suggests that the magnitude of the onshore currents mirrors the magnitude of the wave velocities (cf. Figures 3a and 3b), which is indicative of a wave-driven, streaming phenomenon [*Luhar et al.*, 2010]. During periods of low wave activity, the measured mean currents within the meadow were small, comparable to uncertainty (Figure 4).

[30] Figure 4 compares the measured onshore currents, $-E_{c,m}$, with the model predictions of *Luhar et al.* [2010], given by equation (9) (bold solid line). Also shown are the model predictions accounting for posture asymmetry, based on equation (13) (fine solid line). Both sets of predictions assumed that the ratio of drag coefficients was $C_{Dw}/C_{Dc} = 1$ [*Luhar et al.*, 2010]. The value of the asymmetry parameter, $\epsilon = 0.03$, was chosen to best fit the measured streaming velocities during the high wave periods, by minimizing the sum of squared errors between the

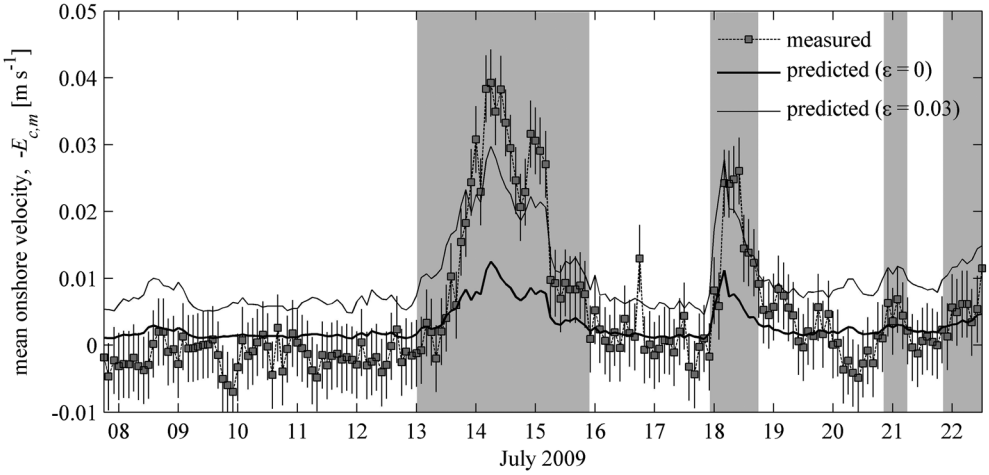

Figure 4. Measured onshore mean velocity, $-E_{c,m}$, during the 2 week deployment. The bold solid line shows the predicted streaming assuming no bias in posture (equation (9)). The fine solid line shows the predicted streaming velocity assuming a 3% bias (equation (13); $\epsilon = 0.03$).

measurements and the predictions. The frequency was calculated from the peak period, $\omega_P = 2\pi/T_P$, and the wave number, k_P, was calculated based on the dispersion relation, $\omega_P^2 = k_P g(\tanh k_P h)$, where g is the acceleration due to gravity. The total wave velocity, $U_{w,m}$, was used to calculate the total streaming velocity in the direction of wave propagation, $|U_{c,m}|$. To estimate the cross-shore streaming velocity, we assumed that the ratio of the cross-shore to total velocity was the same for both the mean and oscillatory components, i.e., $-E_{c,m} = (E_{w,RMS}/U_{w,RMS})U_{c,m}$. In general, the predictions have the same temporal trends as the measurements. However, the magnitude of the streaming is underpredicted by the model assuming zero posture bias, equation (9). Figure 5a, which shows data from the high wave periods, suggests that on average, equation (9) underpredicts the measured currents by a factor of 2.9 during the high wave periods. The predictions accounting for a small posture bias, $\epsilon = 0.03$, perform better during the high wave periods (fine solid line; Figure 4), although note that $\epsilon = 0.03$ overpredicts the streaming flow during the low wave bursts. We provide an explanation for this trend below.

[31] Figure 6a shows the ratio of the oscillatory velocity within and above the meadow, $\alpha = U_{w,m}/U_w$. The full model predictions based on *Luhar et al*. [2010] are also shown in the figure, along with the inertia- and drag-dominated limits, $\alpha_i = 0.87$ and $\alpha_c = 0.05$, given by equations (4) and (5). Given that seagrass blades resemble flexible flat plates, the predictions assumed a flat plate drag coefficient, $C_D = 1.95$. Following *Vogel* [1994], the added mass coefficient was assumed to equal the ratio of blade width (9 mm) to thickness (0.5 mm) for *Posidonia oceanica*, $C_m \approx 18$. The interfacial friction coefficient is expected to be $C_f = O(0.01 - 0.10)$ [*Poggi et al*., 2004; *Lowe et al*., 2005; *Luhar and Nepf*, 2013]. We assumed $C_f = 0.05$ based on the laboratory measurements made by *Ghisalberti and Nepf* [2006] for

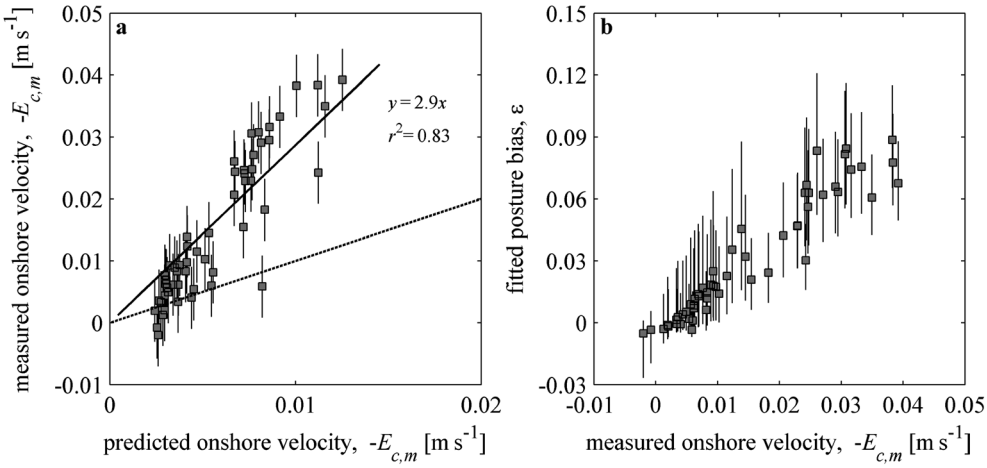

Figure 5. (a) Measured onshore mean velocity plotted against the predictions assuming zero posture asymmetry (equation (9)). The dashed line indicates perfect agreement. The solid line and text correspond to the best-fit line with zero intercept. The error bars reflect instrument uncertainty. (b) Posture bias (ϵ) fitted to the measurements (equation (13), assuming $C_{Dw}/C_{Dc} = 1$) plotted against the measured onshore mean velocity.

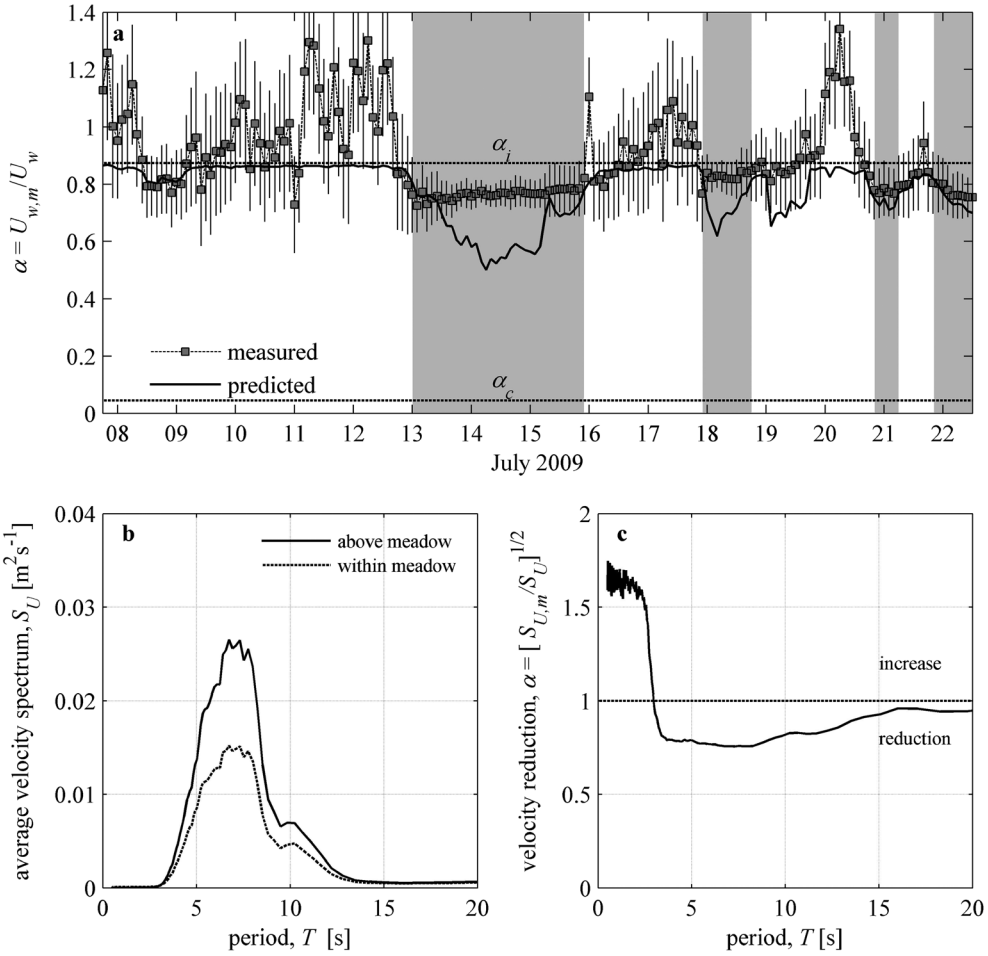

Figure 6. (a) Measured ratio of oscillatory velocity within the meadow to that above the meadow, $\alpha = U_{w,m}/U_w$. Also shown are the predicted ratios based on the theoretical model described in *Luhar et al*. [2010], using a flat plate drag coefficient $C_D = 1.95$ (bold solid line). The inertia and current limits, α_i and α_c (equations (4) and (5)), are shown as horizontal dashed lines. (b) Velocity spectra, averaged over all measurement bursts, measured above and within canopy. (c) Estimated velocity reduction for each spectral component.

unidirectional flows over a submerged meadow of model seagrass.

[32] In agreement with the predictions, the ratio of measured velocities decreased during periods of high wave activity, i.e., as the wave excursion increased and the effects of shear and drag became more pronounced. Averaged over all the high wave bursts, the velocity ratio was $\alpha = 0.78 \pm 0.03$ (mean $\pm$ s.d., $n_b = 55$). Across all bursts, oscillatory velocities within the meadow were reduced by $<30\%$ relative to velocities above the meadow. These data are in broad agreement with the field measurements made by *Koch and Gust* [1999] and *Hansen and Reidenbach* [2012], who showed that wave-induced flows were reduced by 10%–40% within seagrass canopies. During the low wave bursts, the velocity ratio was roughly unity, with $\alpha = 0.95 \pm 0.14$ (mean $\pm$ s.d., $n_b = 123$); i.e., oscillatory velocity within and above the meadow was comparable. However, measurements made during the low wave bursts carried significant uncertainty (as denoted by the error bars in Figure 6a), and so these results must be interpreted with caution. Finally, note that the observed velocity ratios were, in general, larger than the predictions (Figure 6a). For example, when the predicted ratio was lowest, $\alpha = 0.50$ (July 14), the measured ratio was $\alpha = 0.76$. We discuss possible reasons for this difference below.

[33] Figure 6b shows the horizontal velocity spectra, $S_U = S_E + SN$, measured above and within the canopy, averaged over all measurement bursts. In general, the velocity spectra are relatively narrow. Most of the energy is concentrated within the period-band $T = 4$–12 s. There is little or no energy content for $T < 3$ s, which is expected given the natural depth-attenuation of wave orbital velocities. Linear wave theory predicts that the near-bed orbital velocity for waves of period $T = 3$ s in water depth 9 m is $<5\%$ of the velocity at the surface. Note that $T \approx 3$ s also corresponds roughly to the frequency threshold used to limit the velocity spectra for the significant wave height calculations (equation (16)). Figure 6c shows an estimate of the velocity reduction within the canopy across the spectrum, $\alpha = \sqrt{S_{U,m}/S_U}$. For $T = 4$–10 s, the fractional reduction is relatively constant, with $\alpha \approx 0.75$. For $T < 3$ s, there is greater energy content within the canopy relative to that

above the canopy ($\alpha > 1$). This may be attributed to locally generated turbulence within the canopy [*Pujol and Nepf*, 2012]. However, given the generally low energy content at $T < 3$ s (Figure 6b), the estimate of α is prone to error. Finally, the model developed by *Lowe et al.* [2005] and *Lowe et al.* [2007] suggests that the damping of in-canopy flow should increase with wave period (or more accurately, wave excursion). The results shown in Figure 6c do not support this trend. The velocity ratio α estimated for $T > 10$ s is greater than that for $T = 4$–10 s. However, note that the wave-induced streaming flow within the canopy contributes low-frequency content to the velocity spectrum. This could explain the higher α observed for periods $T > 10$ s (Figure 6c).

5. Discussion

[34] Our measurements confirm that a wave-induced streaming flow is generated within natural submerged seagrass meadows. Further, the model developed by *Luhar et al.* [2010] (equation (9)) successfully captures the observed trend; the measured mean current increases with increasing wave amplitude (Figure 4, bold solid line). However, on average, equation (9) underpredicts the measured mean currents by a factor ≈ 2.9 during the high wave periods (Figure 5a). This difference may stem from the fact that velocities were measured at a single point within the meadow, while the model is for depth-averaged quantities. However, we measured velocities at $z \approx 0.5$ m above the bed (or $z/l_v \approx 5/8$), and the laboratory observations made by *Luhar et al.* [2010] suggest that the local streaming velocity at this elevation would be approximately equal to the canopy average. Of course bear in mind that for flexible plants that can be pushed over by the flow, the measurement elevation relative to the seagrass meadow height, z/h_v, is more relevant than the measurement location relative to the blade length, z/l_v. If the real seagrasses were pushed over much more (or much less) by the flow compared to the model plants employed in the laboratory study, the velocity structure observed in the laboratory at $z/l_v \approx 5/8$ may not be representative of that in the field at the same elevation.

[35] The predictions also assume that the measured wave velocity, $U_{w,m}$, equals the canopy average. This assumption, along with any measurement error in $U_{w,m}$, offers another possible explanation for the discrepancy between the measurements and predictions, although equation (9) suggests that $U_{c,m} \propto U_{w,m}^{1.5}$, and based on this scaling, the wave velocity would have to increase by a factor of ≈ 2.0 (200%) to offset the factor ≈ 2.9 underprediction in the measured streaming velocity. This is much larger than any measurement error, which was $<10\%$ during the high wave periods. Further, wave velocities measured above the meadow, U_w, were typically $<30\%$ greater than the velocities measured within the meadow, $U_{w,m}$. Because U_w sets the upper bound for the meadow average, any uncertainty arising from the assumption that $U_{w,m}$ is representative of the meadow average is limited to 30% in the upward direction.

[36] Experimental limitations do not provide a satisfactory explanation for the factor of 2.9 difference between the measured and predicted streaming velocities. Therefore, we suggest that the streaming velocities are underpredicted because equation (9) does not account for a streamwise posture bias similar to that observed by *Luhar et al.* [2010]. The model developed in section 2.3 (equation (13)) shows that the asymmetry in frontal area (and drag) created by this posture bias can strengthen the mean flow significantly. This is confirmed by the predictions based on equation (13) shown in Figure 4 (fine solid line). A small posture bias, $\epsilon = 0.03$ (i.e., frontal area is 3% lower under the wave crest compared to average and 3% higher under the wave trough), results in an increase of ≈ 0.01 m s^{-1} in the magnitude of the predicted streaming velocity. This increase corresponds to roughly 25% of the maximum measured streaming velocity, $|E_{c,m}| \approx 0.04$ m s^{-1}.

[37] However, a constant asymmetry, $\epsilon = 0.03$, does not yield accurate predictions for the streaming flow across all measurement bursts. Using a single, best-fit value for ϵ, the streaming is underpredicted for periods with the most intense wave activity, when the measured velocities were largest, $|E_{c,m}| > 0.03$ m s^{-1} (see 14–15 July; Figure 4). At the same time, $\epsilon = 0.03$ overpredicts the streaming flow during low wave periods where $|E_{c,m}| < 0.01$ m s^{-1}. These observations suggest that the true posture bias is likely to be $\epsilon < 0.03$ during the low wave periods with $|E_{c,m}| < 0.01$ m s^{-1}, and $\epsilon > 0.03$ during the periods with $|E_{c,m}| > 0.03$ m s^{-1}; i.e., the bias increases with the magnitude of the streaming flow. This is confirmed by Figure 5b, which shows the fitted posture bias (calculated from measurements using equation (13), assuming $C_{Dw}/C_{Dc} = 1$) plotted against the measured streaming flow. The fitted posture bias is close to zero for streaming velocities $|E_{c,m}| < 0.01$ m s^{-1} but increases to $\epsilon \approx 0.09$ for $|E_{c,m}| \approx 0.04$ m s^{-1}. This makes physical sense because in the absence of any other mean currents, the posture bias must be generated by the streaming flow itself, i.e., $\epsilon = f(E_{c,m})$, and there is a feedback between the posture bias and the streaming flow. Unfortunately, a more complete characterization of the relationship $\epsilon = f(E_{c,m})$ requires a detailed study of blade-scale dynamics in combined wave-current flows, which is outside the scope of this paper.

[38] Note that equation (9), which assumes zero posture bias, accurately predicted the streaming flow measured by *Luhar et al.* [2010], even though posture asymmetry was present. We suggest a possible explanation for this by considering the relative importance of the wave stress and drag asymmetry terms forcing the mean streaming flow (equation (13)). The relative contribution of the wave stress and drag asymmetry terms depends on the relative magnitude of $(kU_{w,m}/\omega)$ and ϵ. For the laboratory experiments of *Luhar et al.* [2010], the ratio of the oscillatory velocity ($U_{w,m}$) to wave celerity (ω/k) was $kU_{w,m}/\omega = O(0.1)$. Since the model plants employed by *Luhar et al.* [2010] were scaled to be dynamically similar to natural seagrass, we anticipate a drag asymmetry similar to that obtained here, $\epsilon < 0.1$. This value is reasonably consistent with the digital images of plant posture collected during that experiment, which suggest $\epsilon < 0.2$. Therefore, we expect $(kU_{w,m}/\omega) \geq \epsilon$, from which equation (13) suggests that the drag asymmetry was less important than (or comparable to) the wave stress for the laboratory experiments of *Luhar et al.* [2010]. In contrast, for the present field study, $kU_{w,m}/\omega = O(0.01)$, and so $(kU_{w,m}/\omega) < \epsilon$ during the high

wave periods; i.e., the drag asymmetry is the dominant term in equation (13).

[39] Next, we discuss the reduction of wave-induced oscillatory velocities within the seagrass canopy. Figure 6 shows that the measured ratios of oscillatory velocity within and above the meadow, $\alpha = U_{w,m}/U_w$, were consistently higher than the predictions. Again, this difference is likely due to the fact that we do not account for seagrass flexibility. The predictions assumed a rigid, upright morphology, and a flat plate drag coefficient, $C_D = 1.95$. For flexible blades moving with the flow, drag and added mass must be calculated based on the relative velocity and acceleration between the blade and the water. In effect, accounting for flexibility should decrease C_D (increase L_D) relative to that for a rigid flat plate and therefore increase the predicted velocity ratio, which would bring it closer to the observed value.

[40] Note that the assumed value for the drag coefficient, $C_D = 1.95$, is valid only for flat plates in unidirectional currents or at the limit of long wave excursions. *Keulegan and Carpenter* [1958] showed that the drag coefficient for rigid flat plates in oscillatory flows increases as the period parameter (now referred to as the Keulegan-Carpenter number) $KC = U_{w,m}T_P/b$ decreases, i.e., as the wave excursion, $A_{w,m} \sim U_{w,m}T_P$, decreases relative to the plate width, b. For the high wave bursts with $U_{w,m} > 0.05$ m s^{-1} and $T_P > 4.5$ s, we anticipate that $KC > 28$, assuming a typical blade width of $b = 9$ mm. The measurements made by *Keulegan and Carpenter* [1958] suggest that the flat plate drag coefficient is $C_D < 3.3$ for $KC > 28$ and that it approaches a steady value of $C_D \approx 2$ for $KC > 100$. In general, the expression $C_D = 10\,KC^{-1/3}$ represents a reasonable fit to the measurements made by *Keulegan and Carpenter* [1958].

[41] To see how seagrass flexibility reduces the drag coefficient relative to these flat plate values, we extracted C_D by fitting the model to the observed oscillatory velocity reductions, α, during the high wave bursts (shaded gray regions in Figure 6). For the fitting procedure, we employed the full theoretical model for oscillatory velocity reduction developed in *Lowe et al*. [2005] and *Luhar et al*. [2010], for which equations (4) and (5) represent inertia- and drag-dominated limits. Figure 7a shows the fitted drag coefficients (gray squares), together with the values expected for rigid flat plates (bold black line) based on *Keulegan and Carpenter* [1958]. Note that only the fitted drag coefficients with relative uncertainty less than 50% are shown in Figure 7a. As expected, the fitted C_D(=0.48 – 1.5) are lower than the values expected for rigid flat plates ($C_D = 2.0 - 2.8$) over the same range of KC. Further, the fitted C_D decrease faster with increasing Keulegan-Carpenter number, KC, than the flat plate values. The best-fit power law to the observations shows that $C_D \sim KC^{-1.1}$ for the flexible seagrasses, compared to $C_D \sim KC^{-1/3}$ for rigid flat plates. The more rapid decrease in C_D versus KC for the flexible blades may be explained as follows. As KC increases (increasing velocity and period), the flexible seagrass blades move with the flow to a greater degree (i.e., a larger portion of the blade moves nearly passively with the flow). This leads to less drag being generated and a lower effective C_D.

[42] Our measurements suggest a monotonically decreasing relationship between C_D and KC. However, bear in mind that C_D is unlikely to decrease indefinitely with increasing KC. If KC increases to the point where the wave excursion is larger than the blade length, $A_{w,m} > l_v$, or $KC > 2\pi l_v/b$ (≈ 550 for *P. oceanica*), the flexible seagrass blades will spend parts of the wave cycle in a stationary, bent posture. At this limit, where the seagrass blades are nearly stationary, C_D will not decrease further with increasing wave period (increasing KC). Instead, C_D will be set by the stationary, bent posture of the blades, which depends on the blade-scale balance between the hydrodynamic forces pushing the blades over and the forces due to buoyancy or stiffness keeping the blades upright [*Luhar and Nepf*, 2011].

[43] Figure 7a also shows empirically determined relationships, $C_D = f(KC)$, from three previous studies investigating the dissipation of wave energy by submerged seagrass meadows [*Mendez and Losada*, 2004; *Bradley and Houser*, 2009; *Sánchez-González et al*., 2011]. Unfortunately, none of these empirical relationships adequately describe the fitted values of C_D obtained in this study. Further, the C_D predicted by these three relationships differ by more than an order of magnitude. The field measurements of *Bradley and Houser* [2009] suggest that the Reynolds number, $Re = U_{w,m}b/\nu$ (ν is the kinematic viscosity of water), yields better predictions for the drag coefficient, C_D, than the Keulegan-Carpenter number. Figure 7b shows the fitted drag coefficient plotted against the Reynolds number (gray squares), as well as empirical fits, $C_D = f(Re)$, from two previous studies [*Kobayashi et al*., 1993; *Bradley and Houser*, 2009]. In this case, the empirical relationship from *Bradley and Houser* [2009], $C_D = 0.1 + (925/Re)^{3.16}$, represents a reasonable fit to the measurements for α_i. However, note that the power-law component of the relationship obtained by Bradley and Houser, $C_D \sim Re^{-3.16}$, which is dominant for $Re < 1000$ (i.e., $C_D \gg 0.1$), is quite different to that obtained here, $C_D \sim Re^{-1.6}$ (fine solid line in Figure 7b).

[44] To a certain extent, differences between the empirical fits for C_D shown in Figure 7 can be attributed to the fact that the relationships were obtained over different ranges of the Keulegan-Carpenter number, KC, and Reynolds number, Re (see caption for Figure 7). However, the lack of a single, universal relationship of the form $C_D = f(KC)$ or $C_D = f(Re)$ also shows that these empirical fits overlook some important physics. Specifically, they do not consider the effects of plant flexibility, and the ratio of wave excursion to blade length, $A_{w,m}/l_v$. Relative to rigid-body values, the drag coefficients for flexible seagrasses are likely to decrease with increasing plant flexibility or increasing hydrodynamic forcing, as the plants move passively with the flow to a greater degree. So, the relative magnitude of the hydrodynamic forcing and the "restoring" forces due to plant stiffness or buoyancy must also play a role [*Luhar and Nepf*, 2011]. In addition, we call attention to the work of *Denny et al*. [1998] who have considered the interaction between kelp and waves extensively. Specifically, *Denny et al*. [1998] showed that for flexible organisms (e.g., kelp) moving in response to wave-induced unsteady flow, inertial forces can be as important as the forces due to drag, buoyancy, or stiffness. While the drag force depends on the relative velocity between the water and seagrass, inertial forces (e.g., added mass, virtual buoyancy) depend on the acceleration. As a result, large inertial forces can force the flexible seagrass blades to move such that the seagrass blade velocity is no longer in phase with the water velocity. This

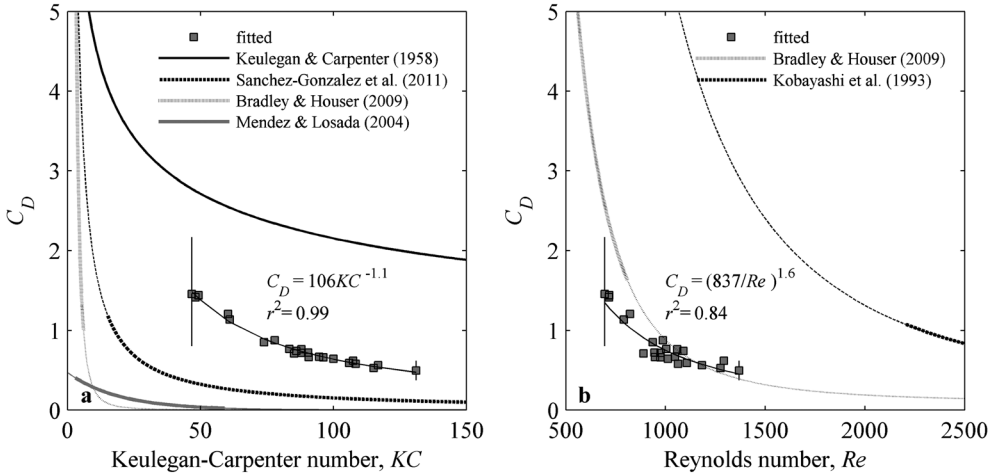

Figure 7. Drag coefficient, C_D, plotted against (a) the Keulegan-Carpenter number, KC, and (b) the Reynolds number, Re. In both plots, the symbols denote values fitted to the measured velocity ratios, α. The errorbars show the typical uncertainty at the highest and lowest C_D. The fine solid lines and text show the best fit power-law relationship for the present study. For comparison, empirical fits for the drag coefficient from previous studies are also shown. Curves shown in Figure 7a: $C_D = 10\ KC^{-1/3}$ based on Keulegan and Carpenter, [1958]; $C_D = 22\ KC^{-1.09}$ from *Sánchez-González et al*. [2011] fitted over $15 < KC < 425$; $C_D = 126\ KC^{-2.7}$ from *Bradley and Houser* [2009] fitted over $1 < KC < 6$; $C_D = 0.47$ exp $(-0.052\ KC)$ from *Mendez and Losada* [2004] fitted over $3 \le KC \le 59$. Curves shown in Figure 7b: $C_D = 0.08 + (2200/Re)^{2.4}$ from *Kobayashi et al*. [1993] fitted over $2200 < Re < 18000$; $C_D = 0.10 + (925/Re)^{3.16}$ from *Bradley and Houser* [2009] fitted over $200 < Re < 800$. In both plots, the bold segments show the range of KC and Re over which the empirical fits were obtained.

phase shift can, in turn, affect the magnitude and the time variation of the drag generated by the seagrass, which sets the energy dissipation within the meadow, the reduction of oscillatory velocity, and the magnitude of the streaming flow generated. Therefore, a comprehensive characterization of seagrass blade motion in oscillatory flow must also account for such inertial effects.

[45] At this point, we must also emphasize that the theoretical models for oscillatory flow reduction and wave-induced streaming discussed in this paper only consider depth-averaged quantities. They do not account for any natural variations in canopy architecture (e.g., frontal area, blade width, and orientation) over the height of the canopy. Since the drag generated by the canopy depends on the frontal area, this natural variation in canopy morphology can create significant variation in flow over the height of the canopy [*Lightbody and Nepf*, 2006]. Therefore, considering the fact that we only measure velocity at one point within the canopy, some of the difference between the measured velocity reduction and the predicted depth-averaged reduction may also be attributed to local variations in canopy drag with height. Finally, note that the simple models used to predict the wave-induced streaming flow (equations (9) and (13)) do not show an explicit dependence on any canopy parameters. However, it is likely that the drag coefficient ratio, C_{Dw}/C_{Dc}, which depends on the size, shape, and motion of the drag-generating elements (i.e., the blades and shoots), varies over the height of the canopy.

[46] As discussed in *Luhar et al*. [2010], the limited reduction of oscillatory velocities within seagrass canopies, and the generation of a streaming flow, could have important environmental implications. By setting the near-bed shear stress, the near-bed velocity plays an important role in controlling sediment suspension. In unidirectional flows, the near-bed velocity and shear stress are significantly reduced due to seagrass canopy drag [*Hansen and Reidenbach*, 2012]. Lower near-bed shear leads to reduced sediment suspension and improved light penetration through the water column. Improved light conditions promote seagrass growth, and the resulting increase in canopy frontal area can lead to further reductions in flow and suspended sediment, creating a positive feedback for seagrass growth. Our results show that in contrast to unidirectional flows, oscillatory flows are not significantly reduced within seagrass canopies. So, the feedback between canopy density and suspended sediment concentrations is likely to be less pronounced.

[47] While seagrass canopies do not significantly damp the local oscillatory flow, they can alter the oscillatory flow over larger distances because they can cause significant wave energy dissipation. A reduction in wave energy leads to smaller waves (i.e., lower wave heights) and reduced oscillatory velocities. For example, *Infantes et al*. [2012] showed that wave heights decreased by 50% over 1000 m of meadow. The wave-induced oscillatory velocity is proportional the wave height, and so, even if seagrass canopies do not significantly damp the local oscillatory flow, the effect of the canopy on wave-induced velocity can be important over larger distances.

6. Conclusions

[48] This field study reveals the presence of a wave-induced mean mass drift in the direction of wave

propagation within seagrass meadows, confirming the laboratory observations of *Luhar et al*. [2010]. With magnitudes as large as 20% of the near-bottom oscillatory velocity, this streaming flow may play an important role in the transport of suspended sediment and organic matter, and dissolved nutrients in vegetated coastal zones. The theoretical model (equation (9)) developed by *Luhar et al*. [2010] underpredicts the magnitude of this mean mass drift by a factor ≈ 3. We suggest this underprediction arises because the previous theoretical model does not account for seagrass motion. Specifically, the presence of the streaming flow is likely to introduce a posture bias, whereby the seagrass blades lean in the direction of wave propagation under the wave crest but remain more upright under the wave trough. Our extension of the model proposed by *Luhar et al*. [2010] shows that the drag asymmetry that results from this posture bias (lower drag under wave crest and greater drag under wave trough) can enhance the streaming flow (equation (13)). The factor ≈ 3 underprediction of the mean mass drift can be reconciled based on a drag asymmetry of $<10\%$, a physically realistic value based on laboratory observations. The theoretical models (equations (9) and (13)) also suggest that the magnitude of the mean mass drift does not depend on the canopy density or relative submergence. However, our measurements, made at a single measurement location (i.e., fixed canopy density and submergence), cannot verify this prediction. Finally, we note that a similar wave-induced mass drift may also exist in other submerged canopies (e.g., macroalgae and coral).

[49] This study also provides further evidence that compared to unidirectional currents, wave-induced oscillatory velocities are not significantly reduced within submerged vegetated canopies. Wave velocity was reduced by $<30\%$ within the submerged meadow relative to the above-meadow velocities, in agreement with previous measurements [*Andersen et al*., 1996; *Koch and Gust*, 1999; *Hansen and Reidenbach*, 2012]. Drag coefficients extracted from the velocity reduction measurements ranged between $C_D \approx 0.5 - 1.5$. The fitted C_D do not agree with the empirical relationships developed in previous studies measuring wave decay over seagrass meadows [*Kobayashi et al*., 1993; *Mendez and Losada*, 2004; *Bradley and Houser*, 2009; *Sánchez-González et al*., 2011]. Further, there is significant disagreement between the individual empirical relationships themselves, all of which assume a Keulegan-Carpenter or Reynolds number dependence, i.e., $C_D = f(KC)$ or $C_D = f(Re)$. We suggest that these differences may be rationalized by accounting for the effects of varying plant flexibility through the use of appropriate dimensionless parameters, e.g., the ratio of hydrodynamic forcing to the restoring force due to plant stiffness [*Luhar and Nepf*, 2011] and the ratio of wave excursion to blade length.

[50] Lastly, sediment suspension rates may vary significantly between seagrass meadows in wave- and current-dominated environments given the vastly different hydrodynamic responses (in-canopy velocity reduction) under wave and current forcing. The suspension, and subsequent transport, of sediment has important engineering (e.g., geomorphic) and ecological (e.g., light penetration, nutrient, and carbon export) implications. So, quantifying sediment suspension rates in seagrass meadows under wave and current forcing is an important next step. This is especially true in light of recent studies which suggest that by trapping organic matter from local (i.e., decaying plant material) and land-based (sediment runoff) sources, seagrass meadows act as important carbon sinks.

[51] **Acknowledgments.** This study received support from the U.S. National Science Foundation under grant OCE 0751358. Any conclusions or recommendations expressed in this material are those of the author(s) and do not necessarily reflect the views of the National Science Foundation. Eduardo Infantes acknowledges financial support received from the Spanish Ministerio de Educacion y Ciencia, FPI scholarship program (BES-2006-12850). We thank the Club Nautico de Cala Bona, which made its harbor facilities available for the field campaign.

References

Andersen, K. H., M. Mork, and J. E. Ø. Nilsen (1996), Measurement of the velocity-profile in and above a forest of *Laminaria hyperborea*, *Sarsia*, *81*(3), 193–196.

Bouma, T. J., M. B. De Vries, E. Low, G. Peralta, C. Tanczos, J. Van de Koppel, and P. M. J. Herman (2005), Trade-offs related to ecosystem engineering: A case study on stiffness of emerging macrophytes, *Ecology*, *86*(8), 2187–2199.

Bradley, K., C. Houser (2009), Relative velocity of seagrass blades: Implications for wave attenuation in low-energy environments, *J. Geophys. Res. -Earth Surf.*, *114*, F01004, doi:10.1029/2007JF000951.

Costanza, R., et al. (1997), The value of the world's ecosystem services and natural capital, *Nature*, *387*(6630), 253–260.

Denny, M., B. Gaylord, B. Helmuth, and T. Daniel (1998), The menace of momentum: Dynamic forces on flexible organisms, *Limnol. Oceanogr.*, *43*(5), 955–968.

Fonseca, M. S., J. A. Cahalan (1992), A preliminary evaluation of wave attenuation by four species of seagrass, *Estuar. Coast. Shelf Sci.*, *35*(6), 565–576.

Gacia, E., T. C. Granata, and C. M. Duarte (1999), An approach to measurement of particle flux and sediment retention within seagrass (*Posidonia oceanica*) meadows, *Aquat. Bot.*, *65*(1-4), 255–268.

Ghisalberti, M., H. Nepf (2006), The structure of the shear layer in flows over rigid and flexible canopies, *Environ. Fluid Mech.*, *6*(3), 277–301, doi:10.1007/s10652-006-0002-4.

Gómez-Pujol, L., A. Orfila, B. Cañellas, A. Alvarez-Ellacuria, F. J. Méndez, R. Medina, and J. Tintoré (2007), Morphodynamic classification of sandy beaches in low energetic marine environment, *Mar. Geol.*, *242*, 235–246.

Hansen, J. C. R., M. A. Reidenbach (2012), Wave and tidally driven flows in eelgrass beds and their effect on sediment suspension, *Mar. Ecol. Prog. Ser.*, *448*, 271–287.

Infantes, E., A. Orfila, G. Simarro, J. Terrados, M. Luhar, and H. Nepf (2012), Effect of a seagrass (*Posidonia oceanica*) meadow on wave propagation, *Mar. Ecol. Prog. Ser.*, *456*, 63–72.

Infantes, E., J. Terrados, A. Orfila, B. Canellas, and A. Alvarez-Ellacuria (2009), Wave energy and the upper depth limit distribution of *Posidonia oceanica* RID B-1062-2008, *Bot. Mar.*, *52*(5), 419–427, doi:10.1515/BOT.2009.050.

Irlandi, E. A., C. H. Peterson (1991), Modification of animal habitat by large plants: mechanisms by which seagrasses influence clam growth, *Oecologia*, *87*(3), 307–318.

Keulegan, G. H., L. H. Carpenter (1958), Forces on cylinders and plates in an oscillating fluid, *J. Res. Natl. Bur. Stand.*, *60*(5), 423–440.

Kobayashi, N., A. W. Raichle, and T. Asano (1993), Wave attenuation by vegetation, *J. Waterw. Port Coastal Ocean Eng. ASCE*, *119*(1), 30–48.

Koch, E. W., G. Gust (1999), Water flow in tide- and wave-dominated beds of the seagrass *Thalassia testudinum*, *Mar. Ecol. Prog. Ser.*, *184*, 63–72.

Lightbody, A. F., H. M. Nepf (2006) Prediction of velocity profiles and longitudinal dispersion in emergent salt marsh vegetation, *Limnol. Oceanogr.*, *51*(1), 218–228.

Lowe, R. J., J. L. Falter, J. R. Koseff, S. G. Monismith, and M. J. Atkinson (2007), Spectral wave flow attenuation within submerged canopies: Implications for wave energy dissipation, *J. Geophys. Res. C: Oceans*, *112*, C05018.

Lowe, R. J., J. R. Koseff, and S. G. Monismith (2005), Oscillatory flow through submerged canopies: 1. Velocity structure, *J. Geophys. Res. C: Oceans*, *110*, C10016.

Luhar, M., S. Coutu, E. Infantes, S. Fox, and H. Nepf (2010), Wave-induced velocities inside a model seagrass bed, *J. Geophys. Res. C: Oceans*, *115*, C12005.

Luhar, M., H. M. Nepf (2013), From the blade scale to the reach scale: A characterization of aquatic vegetative drag, *Adv. Water Resour.*, *51*, 305–316, doi:10.1016/j.advwatres.2012.02.002

Luhar, M., H. M. Nepf (2011), Flow-induced reconfiguration of buoyant and flexible aquatic vegetation, *Limnol. Oceanogr.*, *56*(6), 2003–2017, doi:10.4319/lo.2011.56.6.2003.

Luhar, M., J. Rominger, and H. Nepf (2008), Interaction between flow, transport and vegetation spatial structure, *Environ. Fluid Mech.*, *8*(5-6), 423–439, doi:10.1007/s10652-008-9080-9.

Marbà, N., C. M. Duarte, J. Cebrian, M. E. Gallegos, B. Olesen, and K. Sand-Jensen (1996), Growth and population dynamics of *Posidonia oceanica* on the Spanish Mediterranean Coast: Elucidating seagrass decline, *Mar. Ecol. Prog. Ser.*, *137*(1-3), 203–213.

Mendez, F. J., I. J. Losada (2004), An empirical model to estimate the propagation of random breaking and nonbreaking waves over vegetation fields, *Coast. Eng.*, *51*(2), 103–118.

Nellemann, C., E. Corcoran, C. M. Duarte, L. Valdés, C. De Young, L. Fonseca, and G. Grimsditch (2009), Blue carbon. A rapid response assessment. United Nations Environment Programme, GRID-Arendal, www.grida.no,.

Nepf, H. M. (2012), Flow and transport in regions with aquatic vegetation. *Annu. Rev. Fluid Mech.*, *44*, 123–142.

Poggi, D., A. Porporato, L. Ridolfi, J. D. Albertson, and G. G. Katul (2004), The effect of vegetation density on canopy sub-layer turbulence, *Bound. Layer Meteorol.*, *111*(3), 565–587, doi:10.1023/B:BOUN.0000016576.05621.73.

Pujol, D., and H. Nepf (2012), Breaker-generated turbulence in and above a seagrass meadow, *Cont. Shelf Res.*, *49*, 1–9.

Sánchez-González, J. F., V. Sánchez-Rojas, and C. D. Memos (2011), Wave attenuation due to *Posidonia oceanica* meadows, *J. Hydrau. Res.*, *49*, 503–514.

Sarpkaya, T., M. Isaacson (1981), Mechanics of wave forces on offshore structures.

Thomas, F. I. M., C. D. Cornelisen (2003), Ammonium uptake by seagrass communities: Effects of oscillatory versus unidirectional flow, *Mar. Ecol. Prog. Ser.*, *247*, 51–57.

Vogel, S. (1994), Life in Moving Fluids, Princeton Univ. Press, Princeton, NJ.

Ward, L. G., W. Michael Kemp, and W. R. Boynton (1984), The influence of waves and seagrass communities on suspended particulates in an estuarine embayment, *Mar. Geol.*, *59*(1-4), 85–103.

Zhou, C. Y., J. M. R. Graham (2000), A numerical study of cylinders in waves and currents, *J. Fluids Struct.*, *14*(3), 403–428.